Available online at www.sciencedirect.com
ScienceDirect
Bioelectrochemistry 70 (2007) 311–319
Bioelectrochemistry
www.elsevier.com/locate/bioelechem

Layer-by-layer films of hemoglobin or myoglobin assembled with zeolite particles: Electrochemistry and electrocatalysis

Yi Xie, Hongyun Liu, Naifei Hu *

Department of Chemistry, Beijing Normal University, Beijing 100875, China

Received 20 January 2006; received in revised form 16 March 2006; accepted 11 April 2006
Available online 30 May 2006

Abstract

Positively charged hemoglobin (Hb) or myoglobin (Mb) at pH 5.0 in solutions and negatively charged zeolite particles in dispersions were alternately adsorbed onto solid surfaces forming $\{\text{zeolite/protein}\}_n$ layer-by-layer films, which was confirmed by quartz crystal microbalance (QCM) and cyclic voltammetry (CV). The protein films assembled on pyrolytic graphite (PG) electrodes exhibited a pair of well-defined, nearly reversible CV peaks at about −0.35 V vs. SCE at pH 7.0, characteristic of the heme Fe(III)/Fe(II) redox couples. Hydrogen peroxide (H_2O_2) and nitrite (NO_2^-) in solution were catalytically reduced at $\{\text{zeolite/protein}\}_7$ film modified electrodes, and could be quantitatively determined by CV and amperometry. The shape and position of infrared amide I and II bands of Hb or Mb in $\{\text{zeolite/protein}\}_7$ films suggest that the proteins retain their near-native structure in the films. The penetration experiments of $Fe(CN)_6^{3-}$ as the electroactive probe into these films and scanning electron microscopy (SEM) results indicate that the films possess a great amount of pores or channels. The porous structure of $\{\text{zeolite/protein}\}_n$ films is beneficial to counterion transport, which is crucial for protein electrochemistry in films controlled by the charge-hopping mechanism, and is also helpful for the diffusion of catalysis substrates into the films. The proteins with negatively charged net surface charges at pH 9.0 were also successfully assembled with like-charged zeolite particles into layer-by-layer films, although the adsorption amount was less than that assembled at pH 5.0. The possible reasons for this were discussed, and the driving forces were explored.

Keywords: Layer-by-layer assembly; Zeolite; Hemoglobin; Myoglobin; Direct electrochemistry; Electrochemical catalysis

1. Introduction

Zeolites are a large family of crystalline aluminosilicates organized into regular three-dimensional networks with interconnected channels and cages [1,2]. In recent years, there has been much interest in the applications of zeolite in immobilization of proteins or enzymes since the inorganic zeolite has good biocompatibility, high mechanical, thermal, and chemical stability, large surface areas, and unique hydrophilic and electrostatic property [3–5]. It is well known that the immobilization of enzymes on solid surfaces plays a key role in the development of biosensors, bioreactors and biodevices, and has aroused increasing interest among researchers [6,7].

Zeolite has also been used to immobilize enzymes on electrode surface and construct electrochemical biosensors [8,9]. The direct electrochemistry of some redox proteins at zeolite or molecular-sieve modified electrodes has been realized recently [10–12]. For example, Ju and coworkers investigated the direct electron transfer of cytochrome *c* immobilized on a NaY zeolite matrix and applied the modified electrode in biosensing of hydrogen peroxide [13]. The study on direct electrochemistry of redox enzymes may establish a foundation for fabricating the new type of biosensors without using mediators, and provide a model for the mechanistic study of redox process commonly observed in biological systems [14,15]. Since it is usually difficult for redox proteins in solution phase to transfer electron directly at naked solid electrodes, various types of films have been developed to immobilize proteins on electrode surface, and the direct electrochemistry of the proteins in the film phase has been realized [16,17].

Layer-by-layer assembly, which originated from the alternate adsorption of oppositely charged polyions from their solutions onto solid surfaces, has been developed into a general approach

* Corresponding author. Fax: +86 10 5880 2075.
E-mail address: hunaifei@bnu.edu.cn (N. Hu).

1567-5394/$ - see front matter © 2006 Elsevier B.V. All rights reserved.
doi:10.1016/j.bioelechem.2006.04.002

for fabricating ultrathin films [18–20] and extended to immobilize proteins or enzymes [16,21]. Recently, the direct electrochemistry of redox proteins in layer-by-layer films with polyelectrolytes or nanoparticles has been realized [22–26]. The advantage of layer-by-layer films over cast or dip-coating films is their precisely tailored layer thickness on nanometer scale with predesigned architecture. While the assembly of layer-by-layer films of zeolite with oppositely charged polyelectrolytes has been reported [27–29], to the best of our knowledge, the assembly of layer-by-layer films of zeolite with redox proteins and the direct electrochemistry of the proteins in these films have not been studied yet.

In the present work, hemoglobin (Hb) and myoglobin (Mb) were assembled respectively with zeolite particles by alternate adsorption on solid surfaces, forming $\{\text{zeolite/protein}\}_n$ layer-by-layer films. The $\{\text{zeolite/protein}\}_n$ films grown on pyrolytic graphite (PG) electrodes showed direct and reversible electrochemistry for the protein heme Fe(III)/Fe(II) redox couples, and were characterized by cyclic voltammetry (CV) and square wave voltammetry (SWV). The electrocatalytic reduction of hydrogen peroxide and nitrite were also investigated at $\{\text{zeolite/protein}\}_n$ film electrodes. The structure feature of the films was studied by IR spectroscopy, scanning electron microscopy (SEM) and CV with electroactive probe. The driving forces for the assembly of the films under different conditions were also explored.

2. Experimental section

2.1. Chemicals

Bovine hemoglobin (Hb, MW 66,000) and horse heart myoglobin (Mb, MW 17,800) were purchased from Sigma and used as received. Poly(diallyldimethylammonium chloride) (PDDA, 20%, MW 60,000), poly(sodium 4-styrenesulfonate) (PSS, MW 70,000), and 3-mercapto-1-propanesulfonate (MPS, 90%) were from Aldrich. Zeolite (<45 μm) was purchased from Fluka. All other chemicals were reagent grade. $NaNO_2$ and H_2O_2 were freshly prepared before being used. The water for preparing solutions was purified twice successively by ion exchange and distillation.

2.2. Instruments

A CHI 660A electrochemical workstation (CH Instruments) was used for electrochemical studies. A typical three-electrode cell was used with a saturated calomel electrode (SCE) as the reference electrode, a platinum wire as the counter electrode, and a basal plane pyrolytic graphite (PG, Advanced Ceramics, geometric area 0.16 cm^2) disk modified with films as the working electrode. Buffers were purged with highly purified nitrogen for at least 15 min prior to a series of experiments. A nitrogen environment was then kept in the cell by continuously bubbling N_2 during the whole experiment.

Quartz crystal microbalance (QCM) measurements were done with a CHI 420 electrochemical analyzer. AT-cut quartz resonators (fundamental frequency 8 MHz) coated by thin gold films on both faces (geometric area 0.196 cm^2 per one face) were used. Microscopic reflection absorption infrared (RAIR) spectroscopy was done with a Magna-IR 670 spectrometer (Nicolet). Scanning electron microscopy (SEM) was performed with a JSM-6700F field emission scanning electron microscopy (JEOL). Transmission electron microscopy (TEM) was performed with an H-600 transmission electron microscopy (Hitachi).

2.3. Film assembly

Before being used, zeolite was pretreated with ultrasonication and centrifugation in order to obtain smaller-sized particles with better purity. In brief, the zeolite was dispersed in water at 1 mg mL^{-1} by ultrasonication for about 2 h. After centrifugation at 1500 rpm for 15 min, the supernatant was collected and freeze-dried. TEM showed that sheet-like zeolite had an irregular shape with an average size of about 200 nm at this stage. These purified, smaller-sized particles were then dispersed in buffers at pH 5.0 (3 mg mL^{-1}) by ultrasonication for about 1 h. This cloudy suspension of zeolite was relatively stable. Right before the preparation of zeolite films, the suspension was ultrasonicated for another 15 min.

For electrochemical studies, the basal plane PG electrode was roughened with metallographic sandpaper, and the "edge" surface was uncovered, which was negatively charged by virtue of the surface oxygen functionalities and had a partly hydrophobic character [30]. After immersed into PDDA solutions (3 mg mL^{-1}, containing 0.5 M NaCl) for 20 min, the PG electrode became positively charged owing to the adsorption of PDDA precursor layer. After washed in water, the PG/PDDA electrode was alternately immersed for 20 min in aqueous dispersion of zeolite (3 mg mL^{-1}) and Hb or Mb solutions (3 mg mL^{-1}, containing 0.1 M KCl) at pH 5.0 with intermediate water washing and nitrogen stream drying. This cycle was repeated to obtain the $\{\text{zeolite/protein}\}_n$ layer-by-layer films with the desired number of bilayers (n).

For QCM study, a cleaned gold QCM electrode was immersed in MPS ethanol solutions (4 mM) for 24 h, and an MPS monolayer was formed on gold surface by formation of Au–S bond between Au and MPS, introducing negative charges on the surface. The following assembly of PDDA/$\{\text{zeolite/protein}\}_n$ films on the Au/MPS surface was the same as that on PG. After each adsorption step, the gold QCM electrode was washed in water, dried in N_2 stream, and measured by QCM in air. The $\{\text{zeolite/protein}\}_n$ films on Au QCM electrodes were also used for RAIR spectroscopy and SEM.

3. Results

3.1. Assembly of $\{\text{zeolite/protein}\}_n$ layer-by-layer films

The surface charge of zeolite is dependent on the type of zeolite and the condition in experiments, and usually negative in its dispersions [31]. In our situation, the zeolite would be negatively charged in dispersions according to the experimental results of layer-by-layer assembly of Hb at different pH with the zeolite (see later). With the isoelectric point (pI) at 7.4 for Hb [32] and 6.8 for Mb [33], both Hb and Mb have net positive

surface charges at pH 5.0. Thus, the layer-by-layer films of the zeolite and the proteins were assembled mainly by Coulombic attraction between them, designated as {zeolite/protein}$_n$. QCM and CV were used to monitor or confirm the growth of the films.

QCM can detect tiny mass changes on the QCM resonator electrodes. Based on the Sauerbrey equation [34]

$$\Delta f = -2f_0^2 \Delta m / A(\mu\rho)^{1/2} \quad (1)$$

the frequency shift, Δf (Hz), would be proportional to the adsorbed mass, Δm (g), by taking into account the properties of quartz resonator used in this work, where f_0 is resonant frequency of the fundamental mode of the quartz crystal (8 MHz), μ is the shear modulus of quartz (2.947×10^{11} g cm^{-1} s^{-2}), ρ is the density of the crystal (2.648 g cm^{-3}), and A is the geometric area of the QCM electrode (0.196 cm^2). Thus, 1 Hz of frequency decrease corresponds to 1.35 ng of mass increase. The frequency change or mass increase can also be used to estimate the nominal thickness of adsorbed layer, d (cm), which can be expressed by

$$d = \Delta m / (2\rho_m A) \quad (2)$$

where ρ_m is the density of the layer material (g cm^{-3}). For the protein, the density is estimated to be 1.3±0.1 g cm^{-3} [35], while the density of zeolite is about 2.15±0.15 g cm^{-3} [36]. There are two gold film electrodes coated on both sides of the QCM resonator, the total mass adsorbed on gold QCM electrodes should therefore be divided by 2 in estimation.

QCM results showed a roughly linear decrease in frequency with the adsorption step for both {zeolite/Hb}$_n$ and {zeolite/Mb}$_n$ films grown on Au/MPS/PDDA surfaces (Fig. 1), indicating that the building up of {zeolite/protein}$_n$ films is in a regular and reproducible manner with nearly the same amounts of zeolite and protein in each adsorption bilayer, respectively. The QCM results are listed in Table 1 for comparison. For example, each Hb adsorption layer for {zeolite/Hb}$_n$ films caused a frequency decrease of 449 Hz, larger than that of Mb layer for {zeolite/Mb}$_n$ films (348 Hz), which is qualitatively consistent with the fact that Hb has larger molecular weight than Mb. The nominal thickness of Hb and Mb layer was 11.6 and 9.1 nm, about twice larger than the dimension of Hb ($5.0\times5.5\times6.5$ nm^3 [37]) and Mb

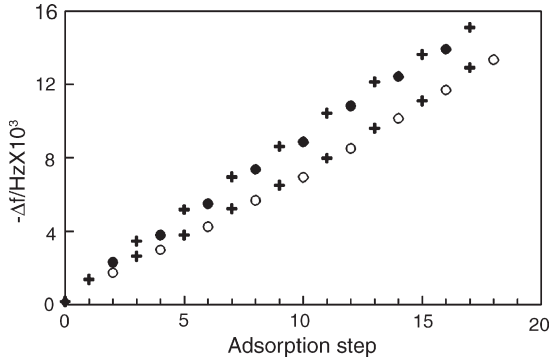

Fig. 1. Dependence of QCM frequency shift on adsorption step for {zeolite/protein}$_n$ films assembled on surface of Au/PDDA/MPS: (♂) MPS/PDDA, (+) zeolite, (○) Hb, and (●) Mb adsorption step.

Table 1
QCM results for each layer of {zeolite/protein}$_n$ films assembled on Au/MPS/PDDA surfaces

Films	Frequency decrease $-\Delta f$, Hz		Nominal thickness d, nm		Γ, mol cm^{-2}
	Zeolite	Protein	Zeolite	Protein	Protein
{zeolite/Mb}$_n$	1189±145	348±59	18.8	9.1	6.7×10^{-11}
{zeolite/Hb(pH 5.0)}$_n$	1059±189	449±68	16.7	11.6	2.33×10^{-11}
{zeolite/Hb(pH 7.0)}$_n$	133±66	185±49	2.1	4.8	0.96×10^{-11}
{zeolite/Hb(pH 9.0)}$_n$	126±50	104±31	2	2.7	0.54×10^{-11}

($2.5\times3.5\times4.5$ nm^3 [38]), respectively, indicating possible aggregation of the proteins in adsorption.

The assembly of {zeolite/protein}$_n$ multilayer films on PG/PDDA surface was also monitored by CV. Taking {zeolite/Hb}$_n$ films as an example, after each adsorption cycle creating a new zeolite/Hb bilayer, the electrode was washed with water and then transferred to a pH 7.0 buffer solution containing no Hb. A pair of well-defined, nearly reversible CV peaks was observed at about −0.35 V vs. SCE (Fig. 2A), characteristic of the Hb heme Fe(III)/Fe(II) redox couples [39]. The reduction and oxidation peak currents grew with the number of zeolite/Hb bilayers (n) until $n=7$. When $n>7$, no further increase in the peak currents was observed, indicating that Hb in the eighth and following bilayers is not electrochemically addressable. {Zeolite/Mb}$_n$ films showed the similar results (Fig. 2B).

3.2. Electrochemical properties

For a specific system, CVs of {zeolite/protein}$_n$ films showed symmetric peak shapes and nearly equal heights of their reduction and oxidation peaks (e.g. Fig. 2), and the heights of the reduction or oxidation peaks were linearly proportional to scan rates from 0.05 to 2.0 V s^{-1}. Integration of reduction peaks at different scan rates in this range gave nearly constant charge (Q) values. All

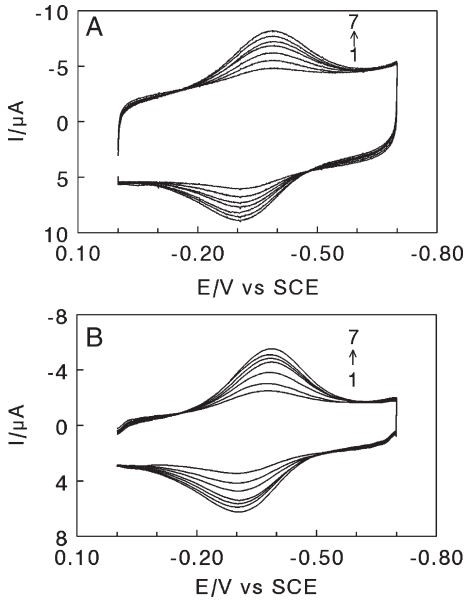

Fig. 2. CVs of (A) {zeolite/Hb}$_n$ and (B) {zeolite/Mb}$_n$ films at 0.2 V s^{-1} in pH 7.0 buffers with different numbers of bilayers (n).

these results indicate the diffusionless, surface-confined electrochemical behavior for the protein film system [40]. Thus, the charge (Q) value by integration of CV reduction peak can be converted to the surface concentration of electroactive protein (Γ^*, mol cm^{-2}) in the films according to the Faraday's law [40], and the fraction of electroactive proteins among the total proteins adsorbed in each bilayer (Γ^*/Γ) can be estimated. Taking {zeolite/Hb}$_n$ films as an example, the surface concentration of electroactive Hb in the first zeolite/Hb bilayer estimated from CV (Γ_1^*) was about 1.65×10^{-11} mol cm^{-2}, while the total surface coverage of Hb in each bilayer measured by QCM (Γ) was about 2.33×10^{-11} mol cm^{-2} (Table 1). The Γ_1^*/Γ ratio for the first bilayer was thus about 71%. The fraction values for the following bilayers were also estimated with the same method. Fig. 3A shows the dependence of the surface concentration (Γ^*) and the fraction of electroactive Hb (Γ^*/Γ) on the number of bilayers (n) for the {zeolite/Hb}$_n$ films. It can be seen that when $n<8$, while the amount of electroactive Hb (Γ^*) increased with n nonlinearly, the Γ^*/Γ ratio decreased with n dramatically. The distance between Hb and the electrode was crucial for efficient electron exchange, and the electroactive Hb could not extend to more than 7 bilayers in this case. The {zeolite/Mb}$_n$ films displayed the similar results (Fig. 3B).

Square wave voltammetry (SWV) combining non-linear regression was used to estimate the apparent heterogeneous electron-transfer rate constant (k_s) and formal potential ($E^{\circ\prime}$) for {zeolite/protein}$_7$ films. The theoretical model was the combination of single-species surface-confined SWV model [41] and the formal potential dispersion model, as described in detail previously [42,43]. The SWV data for {zeolite/protein}$_7$ films showed a good fit on the model over a range of amplitudes and frequencies, and the average k_s and $E^{\circ\prime}$ values estimated are listed in Table 2.

Table 2
Electrochemical parameters of {zeolite/protein}$_7$ films assembled on PG/PDDA electrodes in pH 7.0 buffers

Films	Γ^* [a] (mol cm^{-2})	Γ^*/Γ [a]	ΔE_p [a] (mV)	k_s [b] (s^{-1})	$E^{\circ\prime}$ vs. SCE (V)	
					CV[a]	SWV[b]
{Zeolite/Hb}$_7$	6.04×10^{-11}	44%	88	36.7	−0.347	−0.353
{Zeolite/Mb}$_7$	28.6×10^{-11}	61%	77	35.1	−0.345	−0.358

[a] Data from CVs at 0.2 V s^{-1}.
[b] Data from SWV with average values for analysis of ten SWVs at frequencies of 100–200 Hz, amplitudes of 60–75 mV, and a step height of 4 mV.

The {zeolite/protein}$_7$ films assembled on PG/PDDA electrodes showed very good stability. For example, after 30 days of immersion in pH 7.0 buffers, the peak potentials of {zeolite/Hb}$_7$ films showed no change, and the peak heights decreased only about 10–15% compared with the initial values.

3.3. Electrocatalytic activity

The proteins in {zeolite/protein}$_7$ films demonstrated good electrocatalytic activity toward reduction of hydrogen peroxide and nitrite. For example, the addition of a micro-amount of H_2O_2 into a pH 7.0 buffer caused a large increase in CV reduction peak current for {zeolite/Hb}$_7$ films at −0.4 V, accompanied by the decrease or even disappearance of the oxidation peak (Fig. 4A). No direct reduction peak was observed at PDDA/zeolite film electrode in the presence of H_2O_2. The reduction peak current increased linearly with the concentration of H_2O_2 in solution in a certain range (Table 3). At higher H_2O_2 concentrations, the CV

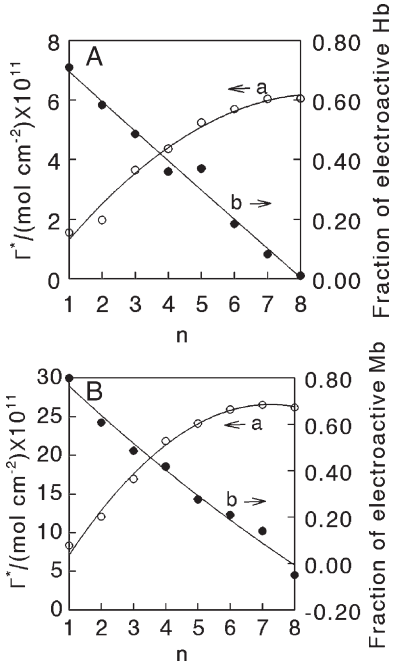

Fig. 3. Influence of the number of bilayers (n) on (a) surface concentration of electroactive proteins (Γ^*) and (b) the fraction of electroactive proteins (Γ^*/Γ) for (A) {zeolite/Hb}$_n$ and (B) {zeolite/Mb}$_n$ films.

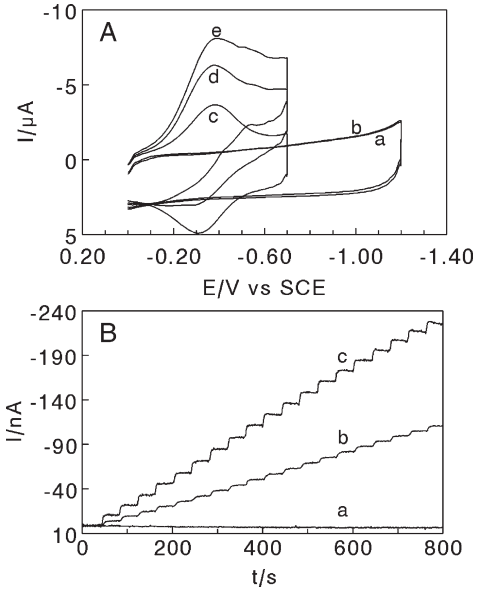

Fig. 4. (A) CVs at 0.2 V s^{-1} in pH 7.0 buffers for (a) PDDA/zeolite film, (b) PDDA/zeolite film in the presence of 30 μM H_2O_2, (c) {zeolite/Hb}$_7$ film, (d) {zeolite/Hb}$_7$ film with 30 μM H_2O_2, and (e) {zeolite/Hb}$_7$ film with 60 μM H_2O_2. (B) Amperometric current–time curves at constant potential of 0 V in pH 7.0 buffers with injection of 50 μM H_2O_2 solution every 40 s for (a) PDDA/zeolite film, (b) {zeolite/Hb}$_7$ film, (c) and {zeolite/Mb}$_7$ film.

Table 3
Electrocatalytic performances of {zeolite/protein}$_7$ films toward reduction of H_2O_2 and $NaNO_2$

Substrate (method)	Films	Linear range (μM)	Correlation coefficient	Detection limit (μM)	Sensitivity (μA μM^{-1} cm^{-2})
H_2O_2 (CV)[a]	{zeolite/Hb}$_7$	0.5–90	0.992	0.05	0.692
	{zeolite/Mb}$_7$	0.5–96	0.994	0.05	0.418
H_2O_2 (RDV)[b]	{zeolite/Hb}$_7$	0.1–15	0.988	0.015	0.818
	{zeolite/Mb}$_7$	0.1–10	0.987	0.015	1.57
H_2O_2 (amperometry)[c]	{zeolite/Hb}$_7$	50–1000	0.995	5	1.02
	{zeolite/Mb}$_7$	50–1000	0.992	5	1.84
$NaNO_2$ (CV)[d]	{zeolite/Hb}$_7$	50–2200	0.996	5	23.5
	{zeolite/Mb}$_7$	50–2400	0.993	5	31.1

[a] In pH 7.0 buffers with scan rate of 0.2 V s^{-1}.
[b] In pH 7.0 buffers with scan rate of 0.05 V s^{-1} and rotation rate of 2000 rpm.
[c] In pH 7.0 buffers at constant potential of 0 V vs. SCE.
[d] In pH 5.0 buffers with scan rate of 0.1 V s^{-1}.

response showed a leveling-off tendency, indicating a typical Michaelis-Menten process [38].

Rotating disk voltammetry (RDV) was also used to investigate the catalytic reduction of H_2O_2 at {zeolite/protein}$_7$ film modified electrodes. Both Hb and Mb in the films demonstrated excellent stability even under the rotating condition. After the addition of H_2O_2, the reduction current increased significantly, and at sufficiently negative potentials, the catalytic current reached the steady state (not shown). The catalytic current at the steady state had a linear relationship with H_2O_2 concentration in solution in a certain range (Table 3).

The electrocatalytic reduction of hydrogen peroxide at {zeolite/protein}$_7$ film electrodes was also studied by amperometry, which is one of the most widely employed techniques for biosensors. The constant potential was set at 0 V vs. SCE after optimization, and the catalytic reduction current was monitored when aliquots of H_2O_2 were added. The stepped increase of H_2O_2 concentration in buffers caused the corresponding growth of catalytic reduction currents (Fig. 4B). In contrast, at the protein-free zeolite film electrode, no current response was observed with the addition of H_2O_2.

The {zeolite/protein}$_7$ films showed good catalytic reactivity for the reduction of nitrite. For instance, the addition of $NaNO_2$ in a pH 5.0 buffer resulted in a new catalytic reduction peak at about −0.7 V for {zeolite/Hb}$_7$ films, while the peak pair at −0.3 V was nearly intact (Fig. 5). This new peak increased with the further addition of nitrite and was used to quantitatively determine the concentration of nitrite in solution (Table 3). Direct reduction of NO_2^- at PDDA/zeolite film electrodes was observed at the potential of more negative than −1.2 V, indicating that the films decrease the reduction overpotential of nitrite by at least 0.5 V.

3.4. Structure features

The shape and position of infrared amide I and II bands may provide detailed information on the secondary structure of polypeptide chains of proteins [44,45]. The amide I band at 1700–1600 cm^{-1} is caused by C=O stretching vibrations of the

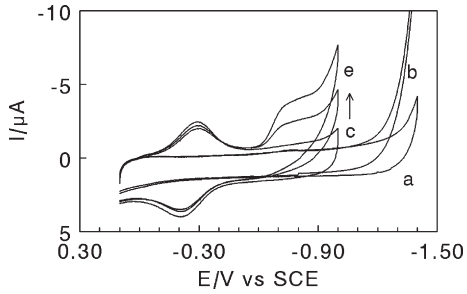

Fig. 5. CVs in pH 5.0 buffers at 0.1 V s^{-1} for (a) PDDA/zeolite film, (b) PDDA/zeolite film with 0.30 mM $NaNO_2$, (c) {zeolite/Hb}$_7$ film, (d) {zeolite/Hb}$_7$ film with 0.30 mM $NaNO_2$, and (e) {zeolite/Hb}$_7$ film with 0.60 mM $NaNO_2$.

peptide linkage and the amide II band at 1600–1500 cm^{-1} is caused by a combination of N–H in-plane bending and C–N stretching of the peptide groups. Microscopic RAIR spectroscopy was thus used to check the two amide bands and corresponding conformational change of proteins in {zeolite/protein}$_7$ films (Fig. 6). For some reasons, the PDDA/zeolite films with no protein incorporated showed some IR absorption in the amide I region and thus interfered the observation of amide I band of the proteins in {zeolite/protein}$_7$ films. However, no peak was observed in the amide II region for the PDDA/zeolite films. Amide II band was therefore used to check the conformation of proteins in the {zeolite/protein}$_7$ films. Both pure Hb and Mb films displayed the amide II band at 1539 cm^{-1}, while {zeolite/Hb}$_7$ and {zeolite/Mb}$_7$ films showed the amide II band at 1536 cm^{-1} and 1541 cm^{-1}, respectively. The peak position and shape of amide II band for {zeolite/protein}$_7$ films were very similar to those for pure corresponding proteins, implying that Hb and Mb retain their near-native structure in the {zeolite/protein}$_7$ films.

The surface morphology of {zeolite/protein}$_7$ films was characterized by SEM. For instance, compared with MPS/PDDA films, the {zeolite/Mb}$_7$ films showed a much rougher surface with many cavities or holes in it (Fig. 7). Similar morphology was also observed for the {zeolite/Hb}$_7$ films (not shown). The porous structure of {zeolite/protein}$_7$ films may allow the small ions in buffers to go through the films very easily, which is beneficial to the electron transfer of proteins in the films with underlying electrodes.

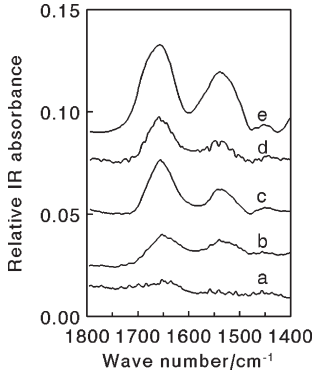

Fig. 6. RAIR spectra for (a) PDDA/zeolite film, (b) {zeolite/Hb}$_7$ film, (c) pure Hb film, (d) {zeolite/Mb}$_7$ film, and (e) pure Mb film.

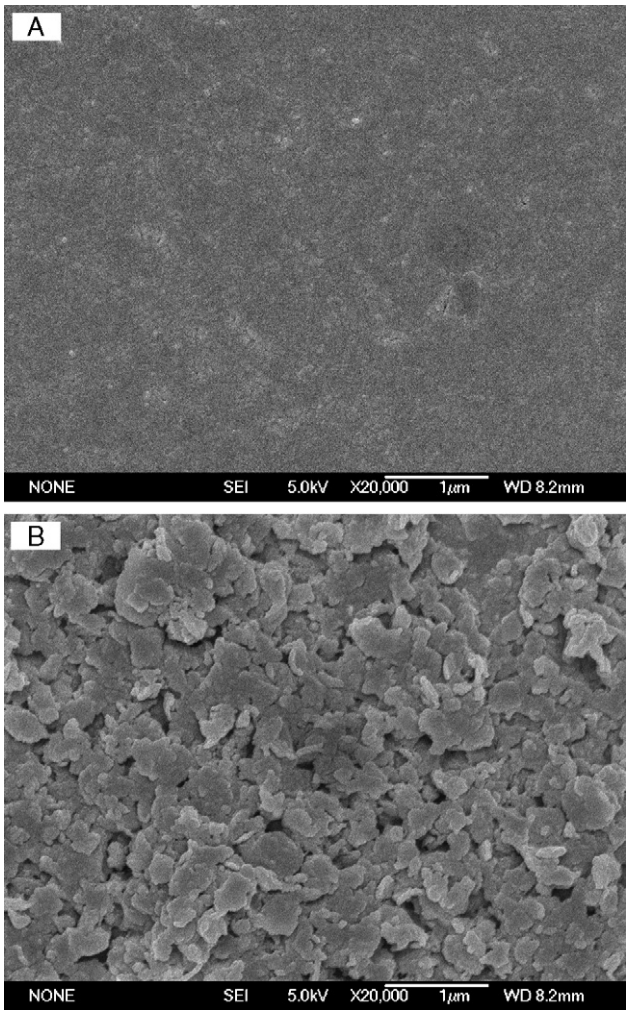

Fig. 7. SEM top view image of (A) MPS/PDDA films on Au substrate and (B) $\{zeolite/Mb\}_7$ films on Au/MPS/PDDA surface.

To further investigate the porosity of $\{zeolite/protein\}_n$ films, CV responses of $Fe(CN)_6^{3-}$ in solution as the electroactive probe were tested with different number of bilayers (n) for $\{zeolite/Mb\}_n$ films. For comparison, the porosity of layer-by-layer films assembled by Mb and poly(styrene sulfonate) (PSS), which was designated as $\{PSS/Mb\}_n$, was also tested by the probe. The well-defined, reversible reduction–oxidation peak pair at about 0.15 V for $Fe(CN)_6^{3-}/Fe(CN)_6^{4-}$ redox couple was observed at PG/PDDA electrodes. When $\{zeolite/Mb\}_n$ or $\{PSS/Mb\}_n$ films were assembled on the PG/PDDA surface, the peak currents for the probe decreased with the number of bilayers (n) and tended to vanish eventually (Fig. 8). This suggests that on one hand, these protein films have some pinholes or channels, which allows the probe ions to go through the films and reach the electrode surface to undergo electron transfer, but on the other hand, the films also have a considerable blocking effect to prevent the probe from approaching the electrode surface. Thicker films showed more pronounced blocking because of the less overall porosity of the films. However, the decrease tendency of the reduction peak current (I_{pc}) of $Fe(CN)_6^{3-}$ with the number of bilayers (n) for $\{zeolite/Mb\}_n$ films was much slower than that for $\{PSS/Mb\}_n$

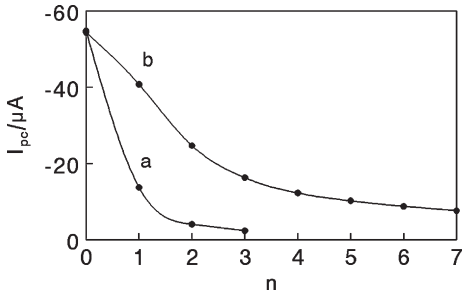

Fig. 8. Dependence of CV reduction peak current (I_{pc}) of 0.5 mM $K_3Fe(CN)_6$ in solutions containing 0.05 M KCl at 0.2 V s^{-1} on the number of bilayers (n) for (a) $\{PSS/Mb\}_n$ and (b) $\{zeolite/Mb\}_n$ films assembled on PG/PDDA electrodes, where $n=0$ corresponds to the PG/PDDA surface.

films (Fig. 8). This suggests that the protein layer-by-layer films made by using zeolite have higher porosity than the films made by using "soft" or flexible polyelectrolyte.

3.5. Driving force study

In the above work, when the $\{zeolite/protein\}_n$ layer-by-layer films were assembled, the pH of the protein adsorbate solution was set at 5.0, and the proteins had net positive surface charges. However, when the pH of the protein adsorbate solution was changed to 7.0 or 9.0, where the proteins were essentially neutral or had net negative surface charges, the layer-by-layer assembly of $\{zeolite/protein\}_n$ films was also realized. Take $\{zeolite/Hb\}_n$ films as an example. The films assembled at different pH were designated as $\{zeolite/Hb(pH\ 5.0)\}_n$, $\{zeolite/Hb(pH\ 7.0)\}_n$, and $\{zeolite/Hb(pH\ 9.0)\}_n$, respectively. The successful assembly of $\{zeolite/Hb(pH\ 7.0)\}_n$ and $\{zeolite/Hb(pH\ 9.0)\}_n$ films were confirmed by QCM (Table 1) and CV (Fig. 9). For QCM experiments, a roughly linear frequency decrease with the number

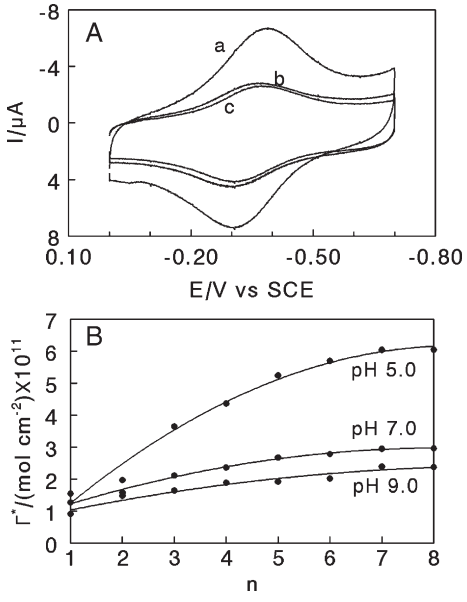

Fig. 9. (A) CVs at 0.2 V s^{-1} in pH 7.0 buffers for (a) $\{zeolite/Hb(pH\ 5.0)\}_7$, (b) $\{zeolite/Hb(pH\ 7.0)\}_7$, and (c) $\{zeolite/Hb(pH\ 9.0)\}_7$ films. (B) Influence of the number of bilayers (n) on surface concentration of electroactive Hb (Γ^*) for $\{zeolite/Hb\}_n$ films assembled at different pH.

of bilayer was observed for {zeolite/Hb(pH 7.0)}$_n$ and {zeolite/Hb(pH 9.0)}$_n$ film systems, respectively, as observed for the {zeolite/Hb(pH 5.0)}$_n$ films. However, the average adsorption amount of Hb and zeolite in each bilayer for {zeolite/Hb(pH 7.0)}$_n$ or {zeolite/Hb(pH 9.0)}$_n$ films was much less than that of {zeolite/Hb(pH 5.0)}$_n$ films, showing the sequence of pH 5.0>pH 7.0>pH 9.0 (Table 1). The results also provided an evidence that the zeolite used in our experiments was negatively charged in its dispersions.

For CV studies, when {zeolite/Hb(pH 7.0)}$_n$ or {zeolite/Hb (pH 9.0)}$_n$ films modified on PG/PDDA electrodes were placed in pH 7.0 buffers, the redox peak pair centered at about −0.35 V for Hb heme Fe(III)/Fe(II) couples was observed, which grew with the number of bilayers (n) up to about 7. Compared with the {zeolite/Hb(pH 5.0)}$_7$ films, the {zeolite/Hb(pH 7.0)}$_n$ or {zeolite/Hb(pH 9.0)}$_n$ films demonstrated much smaller CV peak currents (Fig. 9), in good agreement with the results of QCM. All the {zeolite/Hb}$_n$ films assembled at different pH showed very good stability.

4. Discussion

Heme proteins in {zeolite/protein}$_n$ films showed well-defined, nearly reversible CV peaks for heme Fe(III)/Fe(II) redox couples (Fig. 2) and demonstrated relatively large apparent heterogeneous electron transfer rate constants (k_s, Table 2). Contrarily, Hb and Mb in solution demonstrated poor CV responses at bare PG electrodes. This indicates that zeolite films provide a favorable microenvironment for the proteins and enhance the electron exchange of the proteins with underlying electrodes. The exact mechanism of the enhancement of zeolite for the electron transfer of heme proteins is not very clear yet. However, several factors may play an important role and should be taken into consideration. (1) The good biocompatibility of zeolite [46–48] makes it a good matrix to adsorb proteins and keep their native structures, as IR spectra demonstrated (Fig. 6). (2) The {zeolite/protein}$_n$ films assembled with rigid zeolite have lots of holes or channels in their architecture (Figs. 7 and 8), which allow small inorganic ions in buffers to move into and out of the films more easily, and thus enhance the conductivity of the films and reduce the resistance of charge transfer. (3) The zeolite particles have plenty of interconnected micro-voids inside, and the {zeolite/protein}$_n$ films contain many cavities and channels, all of which may host considerable amounts of water when the films are placed in buffers. This aqueous-like microenvironment may also be favorable for the water-soluble proteins to retain their original structures and transfer electrons with electrodes. (4) The zeolite nanoparticles may have better adsorption selectivity toward the heme proteins than toward the macromolecular impurities originally existing in the protein solution. The repeated adsorption/washing steps in layer-by-layer assembly may be helpful to remove the impurities from the zeolite surface. Thus, the film assembly procedure probably acts as a purification process, and the purified proteins would demonstrate better reversibility at electrodes, as reported in literature [49,50].

The direct electrochemistry of Hb or Mb in cast zeolite films was reported previously [10–13]. However, the present work reports the direct electron transfer of the heme proteins in their layer-by-layer films with zeolite for the first time. The advantage of {zeolite/protein}$_n$ layer-by-layer films over their cast counterparts is the precise control of the film thickness. In addition, the porous zeolite layer provides large surface area with high surface energy, which may adsorb more amounts of proteins in each adsorption step. The QCM results demonstrate that the nominal thickness of protein layer in each adsorption step is about two times larger than the monolayer dimension of the proteins (Table 1). The proteins in {zeolite/protein}$_n$ films display relatively high electroactive fraction in the first few bilayers closest to the electrode surface (Fig. 3). Thus, the utilization efficiency of the proteins in electrochemistry for {zeolite/protein}$_n$ layer-by-layer films would be higher than that of the cast protein films with zeolite. However, when the number of bilayers (n) becomes larger, the fraction of electroactive proteins declines drastically, and after 7 bilayers, the proteins are not electrochemically addressable any more (Fig. 3). The porosity of {zeolite/protein}$_n$ films is also beneficial to the substrate transport within the films in catalysis. The easiness of small H_2O_2 molecules or NO_2^- ions going through the porous films and contacting the proteins results in the low detection limit and good sensitivity in catalytic determination of the substrates (Table 3).

The zeolite particles usually have negative charges in dispersions [31], while the net surface charge of Hb is positive at pH 5.0 with its isoelectric point at pH 7.4 [32]. Thus, the primary driving force for the assembly of {zeolite/Hb(pH 5.0)}$_n$ layer-by-layer films would be electrostatic attraction between oppositely charged zeolite and Hb. However, the assembly of {zeolite/Hb(pH 9.0)}$_n$ multilayer films was also realized when the zeolite and Hb have the same net negative surface charges (Fig. 9). There are two possible explanations for this "counter-intuitive" result. One is the charge inhomogeneity on the protein surface, which results in the localized electrostatic attraction between positively charged groups on Hb surface and negatively charged zeolite. There are considerable amounts of lysine (Lys, pK_a=10–12 [51,52]) and arginine (Arg, pK_a=12–13 [51,52]) residues on Hb surface, which are positively charged even at pH 9.0. Some of these positive groups on Hb surface may be involved in electrostatic interaction with oppositely charged zeolite, giving rise to the assembly of {zeolite/Hb(pH 9.0)}$_n$ films. This explanation was also reported in other layer-by-layer films of proteins with like-charged polyions or nanoparticles [25,26,53]. Another explanation for this "abnormal" result is the charge reversal of Hb when the protein is adsorbed on the zeolite. The negatively charged zeolite layer tends to attract more amounts of H^+ from solution, which may make the pH on zeolite layer surface become much lower than that in bulk Hb adsorbate solution, even leading to the reversal of pH on zeolite surface from higher than pI to lower than pI of Hb. The reversal of net surface charge of amphoteric Hb from negative to positive may make the assembly of {zeolite/Hb (pH 9.0)}$_n$ films become possible. This explanation was reported to be possible according to the theoretical calculation for the adsorption systems of like-charged proteins and polyelectrolytes [54–56]. Both the explanations need to be tested and confirmed by further studies. However, they are all of electrostatic origin. Thus, for both {zeolite/Hb(pH 5.0)}$_n$ and {zeolite/Hb(pH 9.0)}$_n$ films,

the main driving force for the assembly should be the electrostatic interaction between zeolite and Hb, whereas the short-range hydrophobic interactions or/and hydrogen bonding could not be ruled out completely. The successful assembly of {zeolite/Hb(pH 7.0)}$_n$ films, and the sequence of the amount of electroactive Hb at the same n (pH 5.0 > pH 7.0 > pH 9.0) may also be explained by the similar reasons.

5. Conclusions

Zeolite particles with their unique characters were successfully assembled layer-by-layer with heme proteins on solid surfaces mainly by electrostatic interaction. Ordered {zeolite/protein}$_n$ multibilayer films on PG electrodes demonstrated well-defined direct CV responses for heme Fe(III)/Fe(II) redox couples of the proteins and good electrocatalytic activity toward reduction of H_2O_2 and NO_2^-. The {zeolite/protein}$_n$ films demonstrate good porosity, which not only is helpful to the electron transfer of the proteins in the films, but also is beneficial to the mass transport of catalysis substrates through the films. Based on this, {zeolite/protein}$_n$ films show quite high sensitivity in sensing the substrates of environmental or biological significance. The good sensitivity in analysis of the films, combined with the high stability, suggests that the {zeolite/protein}$_n$ layer-by-layer films may have a potential applicability in developing the new type of electrochemical biosensors based on the direct electrochemistry of proteins without using any mediators.

Acknowledgment

The financial support from the National Natural Science Foundation of China (NSFC 20475008 and 20275006) is acknowledged.

References

[1] Y. Ma, W. Tong, H. Zhou, S.L. Suib, A review of zeolite-like porous materials, Microporous Mesoporous Mater. 37 (2000) 243–252.
[2] V. Nikolakis, Understanding interactions in zeolite colloidal suspensions: A review, Curr. Opin. Colloid Interface Sci. 10 (2005) 203–210.
[3] A. Wslvstius, Analytical applications of silica-modified electrodes—a comprehensive review, Electroanalysis 10 (1998) 1217–1235.
[4] J.F. Diaz, K.J. Balkus, Enzyme immobilization in MCM-41 molecular sieve, J. Mol. Catal., B Enzym. 2 (1996) 115–126.
[5] K. Sakaguchi, M. Matsui, F. Mizukami, Applications of zeolite inorganic composites in biotechnology: current state and perspectives, Appl. Microbiol. Biotechnol. 67 (2005) 306–311.
[6] S. Cosnier, Biomolecule immobilization on electrode surfaces by entrapment or attachment to electrochemically polymerized films: A review, Biosens. Bioelectron. 14 (1999) 443–456.
[7] H.A. Heering, F.G.M. Wiertz, C. Dekker, S. de Vries, Direct immobilization of native yeast Iso-1 cytochrome *c* on bare gold: Fast electron relay to redox enzymes and zeptomole protein-film voltammetry, J. Am. Chem. Soc. 126 (2004) 11103–11112.
[8] B. Liu, R. Hu, J. Deng, Fabrication of an amperometric biosensor on the immobilization of glucose oxidase in a modified molecular sieve matrix, Analyst 122 (1997) 821–826.
[9] B. Liu, R. Hu, J. Deng, Characterization of immobilization of an enzyme in a modified Y zeolite to matrix and its application to an amperometric glucose biosensor, Anal. Chem. 69 (1997) 2343–2348.
[10] Z. Dai, H. Ju, H. Chen, Mesoporous materials promoting direct electrochemistry and electrocatalysis of horseradish peroxidase, Electroanalysis 17 (2005) 862–868.
[11] Z. Dai, S. Liu, H. Ju, H. Chen, Direct electron transfer and enzymatic activity of hemoglobin in a hexagonal mesoporous silica matrix, Biosens. Bioelectron. 19 (2004) 861–867.
[12] H. Wang, R. Guan, C. Fan, D. Zhu, G. Li, A hydrogen peroxide biosensor based on the bioelectrocatalysis of hemoglobin incorporated in a kieselgubr film, Sens. Actuators, B, Chem. 84 (2002) 214–218.
[13] Z. Dai, S. Liu, H. Ju, Direct electron transfer of cytochrome *c* immobilized on a NaY zeolite matrix and its application in biosensing, Electrochim. Acta 49 (2004) 2139–2144.
[14] F.A. Armstrong, H.A.O. Hill, N.J. Walton, Direct electrochemistry of redox proteins, Acc. Chem. Res. 21 (1988) 407–413.
[15] M.F. Chapin, C. Bucke, Enzyme Technology, Cambridge University Press, Cambridge, U.K., 1990
[16] J.F. Rusling, in: Y. Lvov, H. Mohwald (Eds.), Protein Architecture: Interfacing Molecular Assemblies and Immobilization Biotechnology, Marcel Dekker, New York, 2000.
[17] F.A. Armstrong, G.S. Wilson, Recent developments in faradaic bioelectrochemistry, Electrochim. Acta 45 (2000) 2623–2645.
[18] G. Decher, Fuzzy nanoassemblies: toward layered polymeric multicomposites, Science 277 (1997) 1232–1237.
[19] N. Kimizuka, M. Tanaka, T. Kunitake, Spatially controlled synthesis of protein/inorganic nano-assembly: alternate molecular layers of cyt. c and TiO_2 nanoparticles, Chem. Lett. 12 (1999) 1333–1334.
[20] Y. Lvov, B. Munge, O. Giraldo, I. Ichinose, S.L. Suib, J.F. Rusling, Films of manganese oxide nanoparticles with polycations or myoglobin from alternate-layer adsorption, Langmuir 16 (2000) 8850–8857.
[21] Y. Lvov, K. Ariga, I. Ichinose, T. Kunitake, Assembly of multicomponent protein films by means of electrostatic layer-by-layer adsorption, J. Am. Chem. Soc. 117 (1995) 6117–6123.
[22] Y. Lvov, Z. Lu, J.B. Schenkman, X. Zu, J.F. Rusling, Direct electrochemistry of myoglobin and cytochrome p450(cam) in alternate layer-by-layer films with DNA and other polyions, J. Am. Chem. Soc. 120 (1998) 4073–4080.
[23] H. Ma, N. Hu, J.F. Rusling, Electroactive myoglobin films grown layer-by-layer with poly(styrensulfonate) on pyrolytic graphite electrodes, Langmuir 16 (2000) 4969–4975.
[24] P. He, N. Hu, G. Zhou, Assembly of electroactive layer-by-layer films of hemoglobin and polycationic poly(diallyldimethylammonium), Biomacromolecules 3 (2002) 139–146.
[25] P. He, N. Hu, J.F. Rusling, Driving forces for layer-by-layer self-assembly of films of SiO_2 nanoparticles and heme proteins, Langmuir 20 (2004) 722–729.
[26] P. He, N. Hu, Interactions between heme proteins and dextran sulfate in layer-by-layer assembly films, J. Phys. Chem., B 108 (2004) 13144–13152.
[27] G.S. Lee, Y.J. Lee, K.B. Yoon, Layer-by-layer assembly of zeolite crystals on glass with polyelectrolytes as ionic linkers, J. Am. Chem. Soc. 123 (2001) 9769–9779.
[28] X. Wang, W. Yang, Y. Tang, Y. Wang, S. Fu, Z. Gao, Fabrication of hollow zeolite spheres, Chem. Commun. 21 (2000) 2161–2162.
[29] V. Hornok, A. Erdohelyi, I. Dekany, Preparation of ultrathin membranes by layer-by-layer deposition of layered double hydroxide (LDH) and polystyrene sulfonate (PSS), Colloid Polym. Sci. 283 (2005) 1050–1055.
[30] H.A.O. Hill, Bio-electrochemistry, Pure Appl. Chem. 59 (1987) 743–748.
[31] M. Masayoshi, K. Yoshimichi, Y. Taichi, M. Yoshiyuki, M. Fujio, S. Kengo, Selective adsorption of biopolymers on zeolites, Chem. Eur. J. 7 (2001) 1555–1560.
[32] J.B. Matthew, G.I.H. Hanania, F.R.N. Gurd, Electrostatic effects in hemoglobin-hydrogen-ion equilibria in human deoxyhemoglobin and oxyhemoglobin-A.104. Biochemistry 18 (1979) 1919–1928.
[33] A. Bellelli, G. Antonini, M. Brunori, B.A. Springer, S.J. Sligar, Transient spectroscopy of the reaction of cyanide with ferrous myoglobin—effect of distal side residues, J. Biol. Chem. 265 (1990) 18898–18901.
[34] G. Sauerbrey, Verwendung von schwingquarzen zur wagung schichten und zur mikrowagung, Z. Phys. 155 (1959) 206–222.
[35] T.E. Creighton, Protein Structure, a Practical Approach, IRL Press, New York, 1990.

[36] Research Group on Molecular Sieves in Dalian Institute of Chemical Physics, Chinese Academy of Sciences, Zeolite and Molecular Sieves, Science Press: Beijing, 1978.
[37] M. Perutz, H. Muirhead, J. Cox, L. Goaman, L. Mathews, E. McGandy, L. Webb, Three-dimensional fourier synthesis of horse oxyhaemoglobin at 2.8 Å resolution (1) X-ray analysis, Nature 219 (1968) 29–32.
[38] L. Stryer, Biochemistry, 3rd ed. Freeman, New York, 1988.
[39] Q. Huang, Z. Lu, J.F. Rusling, Composite films of surfactants, nation, and proteins with electrochemical and enzyme activity, Langmuir 12 (1996) 5472–5480.
[40] R.W. Murray, in: A.J. Bard (Ed.), Electroanalytical Chemistry, vol. 13, Marcel Dekker, New York, 1984, pp. 191–368.
[41] J.J. O'Dea, J.G. Osteryoung, Characterization of quasi-reversible surface processes by square-wave voltammetry, Anal. Chem. 65 (1993) 3090–3097.
[42] A.-E.F. Nassar, Z. Zhang, N. Hu, J.F. Rusling, T.F. Kumosinski, Proton-coupled electron transfer from electrodes to myoglobin in ordered biomembrane-like films, J. Phys. Chem., B 101 (1997) 2224–2231.
[43] Z. Zhang, J.F. Rusling, Electron transfer between myoglobin and electrodes in thin films of phosphatidylcholines and dihexadecylphosphate, Biophys. Chem. 63 (1997) 133–146.
[44] A. Dong, P. Huang, W.S. Caughey, Protein secondary structures in water from 2nd-derivative amide-I infrared-spectra, Biochemistry 29 (1990) 3303–3308.
[45] J.F. Rusling, T.F. Kumosinski, Nonlinear Computer Modeling of Chemical and Biochemical Data, Academic Press, New York, 1996.
[46] C.H. Lee, J. Lang, C.W. Yen, P.C. Shih, T.S. Lin, C.Y. Mou, Enhancing stability and oxidation activity of cytochrome *c* by immobilization in the nanochannels of mesoporous aluminosilicates, J. Phys. Chem., B 109 (2005) 12277–12286.
[47] Y. Wang, F. Caruso, Macroporous zeolitic membrane bioreactors, Adv. Funct. Mater. 14 (2004) 1012–1018.
[48] E. Dumitriu, F. Secundo, J. Patarin, L. Fechete, Preparation and properties of lipase immobilized on MCM-36 support, J. Mol. Catal., B Enzym. 22 (2003) 119–133.
[49] T. Daido, T. Akaike, Electrochemistry of cytochrome *c*: influence of coulombic attraction with indium tin oxide electrode, J. Electroanal. Chem. 344 (1993) 91–106.
[50] I. Taniguchi, K. Watanabe, M. Tominaga, F.M. Hawkridge, Direct electron transfer of horse heart myoglobin at an indium oxide electrode, J. Electroanal. Chem. 333 (1992) 331–338.
[51] A.S. Yang, B.J. Honig, Structural origins of pH and ionic-strength effects on protein stability—acid denaturation of sperm whale apomyoglobin, Mol. Biol. 237 (1994) 602–614.
[52] S.J. Shire, G.I.H. Hanania, F.R.N. Gurd, Electrostatic effects in myoglobin hydrogen ion equilibria in sperm whale ferrimyoglobin, Biochemistry 13 (1974) 2967–2974.
[53] J.B. Schenkman, I. Jansson, Y.M. Lvov, J.F. Rusling, S. Boussaad, N.J. Tao, Charge-dependent sidedness of cytochrome p450 forms studied by quartz crystal microbalance and atomic force microscopy, Arch. Biochem. Biophys. 385 (2001) 78–87.
[54] P.M. Biesheuvel, M.A.C. Stuart, Electrostatic free energy of weakly charged macromolecules in solution and intermacromolecular complexes consisting of oppositely charged polymers, Langmuir 20 (2004) 2785–2791.
[55] A. Wittemann, B. Haupt, M. Ballauff, Adsorption of proteins on spherical polyelectrolyte brushes in aqueous solution, Phys. Chem. Chem. Phys. 5 (2003) 1671–1677.
[56] P.M. Biesheuvel, A. Wittemann, A modified box model including charge regulation for protein adsorption in a spherical polyelectrolyte brush, J. Phys. Chem., B 109 (2005) 4209–4214.